6019

International Symposium on Room Air Convection and Ventilation Effectiveness
University of Tokyo, July 22 – 24, 1992

NUMERICAL SIMULATION OF INDOOR AIR TEMPERATURE AND WALL HEAT FLOW DISTRIBUTION OF A HEATED AND COOLED ROOM

TAKEMASA Yuichi
Kajima Technical Research Institute, 2–19–1, Tobita–kyu, Chyohu City, Tokyo 182, Japan

KURABUCHI Takashi
Lecturer, Dept. of Architecture, Faculty of Eng., Science Univ. of Tokyo, 1–3, Kagurazaka, Shinjuku–ku, Tokyo 162, Japan

KAMATA Motoyasu
Asoc. Prof., Dept. of Architecture, Faculty of Eng., Univ. of Tokyo, 7–3–1, Hongo, Bunkyo–ku, Tokyo 113, Japan

ABSTRACT
Numerical simulation has been becoming reliable for predicting detailed indoor airflow and gaseous contaminant distribution under isothermal conditions. However, application to actual cooling and heating has been restricted, partially due to the uncertainty of deriving wall heat flow from wall surface temperature. For this report, a three–dimensional numerical study based on the k–ε turbulence model was conducted with wall function method in order to determine the accuracy and applicability of the current numerical schemes for predicting indoor air distribution and convective wall heat flows. Calculations were conducted using three types of wall functions and three different mesh intervals in the vicinity of a wall, and the accuracy of each was evaluated by comparisons with full–scale–model experiments. It is demonstrated that a wall function which depends on the turbulence energy at wall adjacent node and takes into account viscous sublayer thickness produces the most satisfactory results.

KEYWORDS
numerical simulation, indoor airflow, full–scale–model experiment, convective heat flows, convective heat transfer coefficient

INTRODUCTION
Accurate evaluation of wall heat flows is an essential part of predicting the air distribution of an air–conditioned room, because wall heat flows can directly affect indoor air temperature and so its buoyancy force. Many previous studies have been conducted to develop reliable wall boundary conditions in order to estimate wall heat flows. Recently, a method which uses extremely fine mesh in the vicinity of a wall and a turbulence model which takes account of the low–Reynolds–number effect was presented and applied to flows in simple two–dimensional geometries [Patel et al., 1984]. This approach directly employs wall surface temperature and velocity as wall boundary conditions, so it is not necessary to assume their near–wall distributions. In spite of these superior characteristics, its application to general engineering flows seems to be limited due to the uncertainty of the low–Reynolds–number turbulence model and heavy computational demands. Alternatively, the wall function approach, which bridges the gap between wall surface and wall adjacent node based on the boundary layer theory, is still a practical choice at the present stage of development.
In this report, airflow and wall heat flow distribution is predicted for an air–conditioned room using three wall functions. The results are compared with the corresponding full–scale–model experiments, and the applicability of each scheme is discussed.

FULL–SCALE–MODEL–EXPERIMENTS
Experiments were performed using a full–scale empty room model 3.0 m wide, 3.0 m long, and 2.5 m high. The room model was constructed of insulated boards and a glass sheet to form a perimeter zone as illustrated in Figure 1. A supply air inlet nozzle measuring 0.15 m by 0.15 m

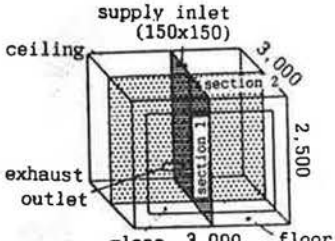

walls, ceiling:
particle board (12 mm)
+ insulated board (75 mm)
+ particle board (12 mm)
floor: particle board (12 mm)
+ insulated board (75 mm)
+ particle board (12 mm)
glass: 5 mm

FIGURE 1 Room Geometry

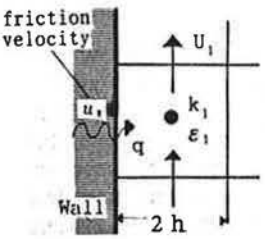

FIGURE 3 Symbols in a Wall Adjacent Cell

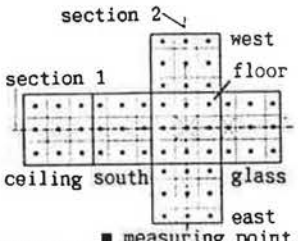

FIGURE 2 Location of Measuring Points of Transmission Heat Flows and Wall Surface Temperatures

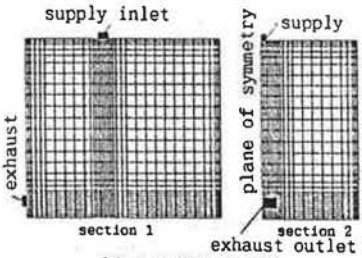

Mesh 2 (28x34x20)

Mesh 1: 26x32x19. Wall adjacent mesh interval is 7.5 cm.
Mesh 2: 28x34x20. Wall adjacent mesh interval is 3.75 cm.
Mesh 3: 32x38x22. Wall adjacent mesh interval is 0.9375 cm.

FIGURE 4 Mesh Layout

TABLE 1 Test Conditions and Total Heat Balances

test	C07	C10	C15	H07	H12	H15
cooling/heating	cool	cool	cool	heat	heat	heat
air change rate (1/h)	7	10	15	7	12	15
Reynolds number (10^{-4})	1.95	2.78	4.18	1.95	3.34	4.27
Archimedes number (10^{-4})	1.52	.638	.231	1.59	.374	.200
transmission heat flows (kcal/h)	550	666	801	582	687	762
total heat loss/gain (kcal/h)	519	632	775	542	639	713
heat balance error (%)	5.9	5.5	3.4	7.4	7.5	6.9

was located in the ceiling, and an exhaust outlet 0.15 m by 0.45 m was situated on a wall close to the floor. The heat input and outpt of the room was controlled by the air temperature of the airflow laboratory surrounding the model, and no internal heat load was assumed. Six different steady-state cooling and heating cases were tested by controlling supply air volume, supply air temperature and the surrounding air temperature. The principal measuring points were for the air temperatures (90 points), wall transmission heat flows (54 points), and corresponding surface temperatures as illustrated in Figure 2. All temperatures and wall transmitted heat flows were measured by thermocouples (0.2 mmϕ) and heat flow sensors with data acquisition systems. The test conditions and the results of total heat balances are given in Table 1. As shown in the Table, heat balance error, 1-(transmisson heat)/(total convective heat loss or gain) was within 10% in each case, and thus the data may be considered accurate enough for quantitative comparisons with simulations of the wall heat flow distribution.

CALCULATION PROCEDURE AND BOUNDARY CONDITIONS

Numerical simulation, correponding to the experiment case C10 of cooling and case H12 of heating,

TABLE 2 Wall Boundary Conditions

- Type 0
  q : experimental value
  Other boundary conditions are the same as Type 3.
- Type 1 (based on $Re_\lambda = U_1 h/\nu$)

$$u_* : \left(\frac{u_*}{U_1}\right)^2 = \begin{cases} 1/Re_\lambda & Re_\lambda \leq 25 \\ 1.829/(ln\,Re_\lambda)^{3.270} & 25 < Re_\lambda \leq 420 \\ .1464/(ln\,Re_\lambda)^{1.866} & 420 < Re_\lambda \end{cases}$$

k : $k_1 = C_D^{-1/2} u_*^2$, ε : $\varepsilon_1 = u_*^3/(\kappa h)$
q : $q/(C_p\rho) = u_*^2/(\sigma_t U_1)\cdot(\theta_w - \theta_1)$
where $\sigma = \sigma_t = 0.7$ is assumed.

- Type 2 (based on $Re_* = v_* h/\nu$)

$$u_* : \frac{U_1 v_*}{u_*^2} = \begin{cases} Re_* & Re_* \leq 5 \\ 5.0\,ln(Re_*) - 3.05 & 5 < Re_* \leq 30 \\ 2.5\,ln(Re_*) + 5.50 & 30 < Re_* \end{cases}$$

k : $(\partial k/\partial z)_w = 0$, ε and q : same as Type 1
where $v_* = C_D^{1/4} k_1^{1/2}$: velocity scale introduced by Launder & Spalding [1974].

- Type 3 (see references [Chien & Launder, 1980])

u_* : $u_*^2 = \kappa w_* U_1/[ln(2w_* hE/\nu) + \lambda - 1 - \kappa w_* \lambda z_0/(2\nu)]$
k, ε and q : same as Type 2
turbulent production terms for wall adjacent cell are
stress production : $P_1 = u_*^4/(2\kappa w_* h)\cdot ln(1/\lambda)$
buoyancy production :
$G_1 = g\beta q(1-\lambda)/(C_p\rho)$ (horizontal wall)
$G_1 = 0$ (vertical wall)
dissipation : $\varepsilon_1 = 2\nu k_0/(4\lambda h^2) + C_D^{3/4} k_0^{3/2}/(2\kappa h)\cdot ln(1/\lambda)$
where $w_* = C_D^{1/4} k_0^{1/2}$: velocity scale introduced by Chien & Launder , k_0: turbulent kinetic energy in turbulent region, z_0: viscous sublayer thickness, E : 9.0, empirical constant, $\lambda = z_0/(2h)$: volumetric share of viscous sublayer at wall adjacent cell, κ : 0.4, Karman constant.

was conducted by means of the Viollet type buoyancy extended k–ε turbulence model [Viollet, 1987] and the ABMAC finite-difference procedure [Viecelli, 1971].

As a preliminary part of the study, indoor airflow and air temperature distribution were to be calculated based on the experimentally determined wall convective heat flows, which were estimated using the absorption factor method [Gebhalt, 1959] by processing the measured wall surface temperatures and wall transmitted heat flows. Then, the wall boundary condition was changed to the wall surface temperature type, and the wall convective heat flows were internally generated using wall functions. As shown in Table 2, three types of wall functions were examined to evaluate their applicability to the actual air-conditioning situations.

Type 1 relates local heat transfer coefficient to the resultant velocity component tangential to walls at wall adjacent node [Kaizuka and Kajiya, 1983, Kurabuchi and Kamata, 1989]. Type 2 is a version of the generalized log-law [Launder and Spalding, 1974, Kurabuchi and Kamata, 1989], and is dependent on the wall adjacent turbulent kinetic energy. Type 3 is a simplified form of the near-wall model for high Reynolds numbers [Chieng and Launder, 1980, Takemasa et al., 1990], and the viscous sublayer effects are taken into consideration (for symbols used in Table 2, see Figure 3). As for the mesh resolution near walls, the three types shown in Figure 4 were tested to evaluate the grid dependency of wall convective heat flows.

CALCULATIONS BASED ON IMPOSED WALL CONVECTIVE HEAT FLOWS

Results of simulation calculations of the cooling and heating air-conditioning cases (C10 and H12) based on Mesh 2 are shown in Figures 5 and 6 for the representative planes (see Figure 1), where calculated velocity vectors are presented and temperature profiles at measured locations are compared with experiment results. According to the airflow pattern of the cooling case (Figure 5(a)), the downward cold jet together with the upward buoyant convection near the glass surface forms a large anti-clockwise recirculation. In the heating case (Figure 6(a)), a hot radial wall jet after impinging the floor is pushed back by the cold draught down the glass surface and forms complicated airflows near the floor. Unfortunately, there are no data with which to compare them. Indoor air temperature is slightly underestimated by about 0.1 in the upper part of the room in the cooling case (Figure 5(b)), and is overestimated near the jet region in the heating case (Figure 6(b)). However, the general features of indoor air temperature distribution are well reproduced.

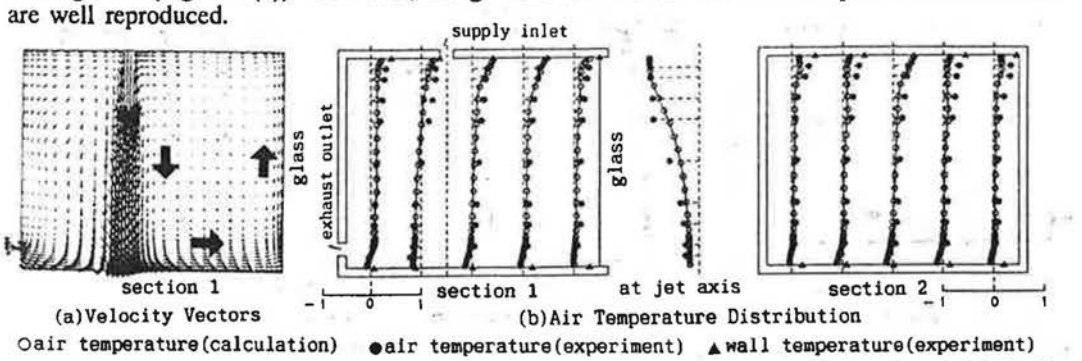

FIGURE 5 Calculated Results Based on Evaluated Wall Convective Heat Flows (C10, Type 0, Mesh 2)

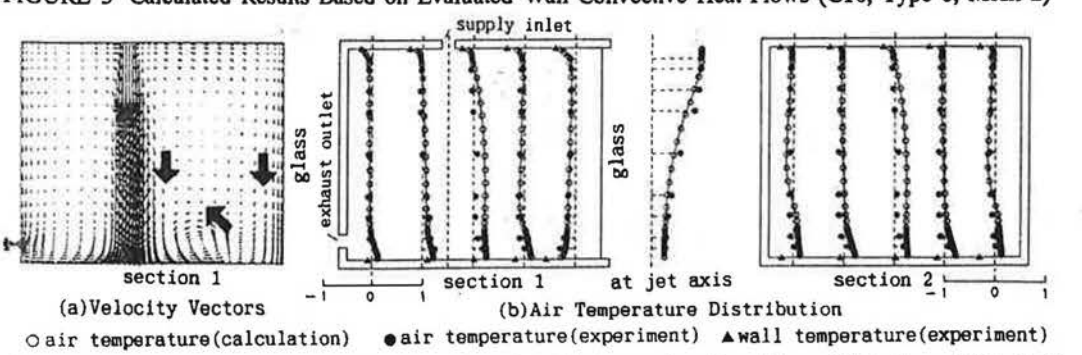

FIGURE 6 Calculated Results Based on Evaluated Wall Convective Heat Flows (H12, Type 0, Mesh 2)

CALCULATIONS BASED ON WALL SURFACE TEMPERATURE

Calculations were carried out for Mesh 2 (see Figure 4) based on the measured wall surface temperature and wall functions. The simulated wall heat flow distributions of each wall function are summarized in Table 3 (1),(2),(4) for the cooling case, and Table 4 (1),(2),(4) for the heating case. In this Table, total convective heat flows through each wall, ceiling and floor are presented as a relative magnitude to the measured total heat loss or gain and are compared to the values obtained in experiments.

The experiment results indicate that the ceiling heat flows are markedly different between the heating and the cooling cases. The total heat flows of the heating case are almost three times as large as the cooling case, apparently due to the different heat flow direction. Type 2 and 3 wall functions reproduce this trend, at least qualitatively. In Type 1 results, no noticeable difference is observed between the heating and cooling cases. This discrepancy is probably due to the

TABLE 3 Calculated and Observed Wall Convective Heat Flows (C10)

	ceiling	floor	east	west	south	glass	total
experiments	4.8	28.6	13.1	12.3	10.7	30.5	100.0
(1) Type 1, Mesh 2	10.1	17.8	10.5	10.5	9.3	27.8	85.9
(2) Type 2, Mesh 2	8.6	23.3	10.2	10.2	11.0	27.3	90.4
(3) Type 3, Mesh 1	10.8	21.8	10.8	10.8	10.0	28.1	92.4
(4) Type 3, Mesh 2	7.4	22.2	10.4	10.4	10.2	33.0	93.6
(5) Type 3, Mesh 3	6.9	21.3	11.1	11.1	12.0	34.8	97.2

TABLE 4 Calculated and Observed Wall Convective Heat Flows (H12)

	ceiling	floor	east	west	south	glass	total
experiments	16.3	21.4	12.7	12.0	12.0	25.5	100.0
(1) Type 1, Mesh 2	11.1	17.7	8.5	8.5	9.2	21.9	77.0
(2) Type 2, Mesh 2	13.1	25.3	8.7	8.7	10.1	21.7	87.6
(3) Type 3, Mesh 1	13.2	23.5	9.1	9.1	10.6	23.6	89.0
(4) Type 3, Mesh 2	13.1	23.5	8.2	8.2	10.7	25.4	89.0
(5) Type 3, Mesh 3	13.2	21.2	8.4	8.4	11.0	27.2	89.4

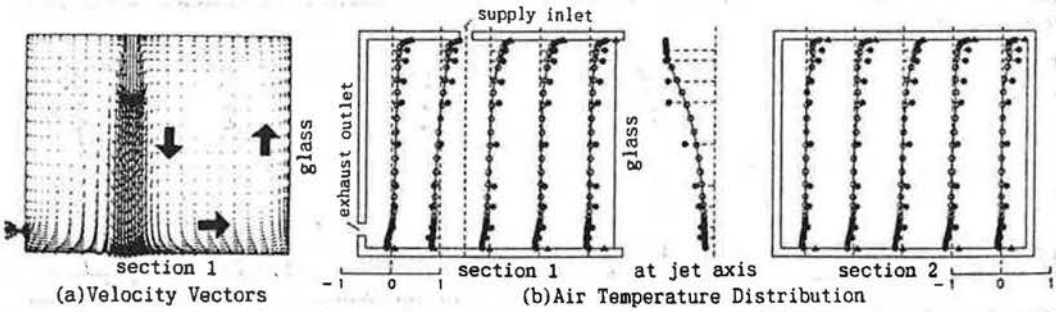

FIGURE 7 Calculated Results Based on Measured Wall Surface Temperature (C10, Type 3, Mesh 3)

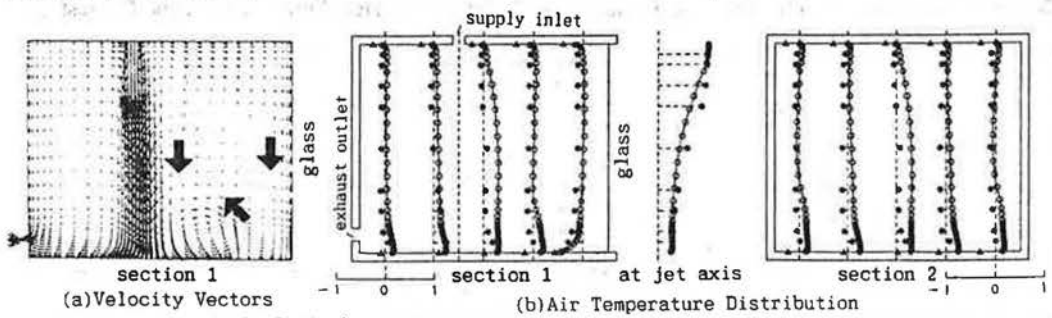

FIGURE 8 Calculated Results Based on Measured Wall Surface Temperature (H12, Type 3, Mesh 3)

absence of the buoyancy effect in the near-wall model in Type 1. Underestimation of heat flows in Type 1 is also apparent in the impinging region of the floor for the cooling case. This disagreement is caused by the small radial component of velocity near the center of jet impinging. On the other hand, the results of Type 2 and 3 are in good agreement with the experiment results, and these suggest the possibility of the local convective heat transfer coefficients being well correlated with the turbulence energy. As for the total heat loads, Type 3 gives slightly better agreement than Type 2, with Type 1 a poor third.

Grid dependency tests were made only for the Type 3 wall function. The simulated heat flow results of three mesh layouts are summarized in Table 3 (3),(4),(5) for the cooling case and Table 4 (3),(4),(5) for the heating case. The calculated total heat loads are slightly smaller than the experiment results, ranging from 89 to 97% of observed values. As the wall adjacent mesh size becomes smaller, closer agreement with the experiment results is obtained both for the cooling and heating cases. However, the convective heat flow calculated by Type 3 is not greatly sensitive to the near-wall mesh size because the variations of mesh sizes ranging from 7.5 cm to 0.9375 cm provide different total heat loads of 4.8% and 0.4% for the cooling and heating cases, respectively. This suggests that the volumetric share of a viscous sublayer at a wall adjacent cell, λ ($=z_0/2h$) taking values of 0.1–0.3 for Mesh 2 and 0.6 for Mesh 3, effectively dumps excessive amounts of turbulence production for fine mesh cases. Calculated velocity vectors and temperature distribution for the finest Mesh 3 are presented in Figures 7 and 8. The velocity vectors shown in Figures 7 and 8 are in close agreement with those in Figures 5 and 6. The air temperature distribution of the cooling case also shows good agreement with Figure 5 and with the experiment data, but slight overestimation is observed in the heating case caused by the total heat load error.

Calculated distributions of convective heat flow, q kcal/m^{2}h, are shown and compared to the experiment data in Figures 9 and 10 for the cooling and heating case, respectively. Convective heat transfer coefficients, α_c kcal/m^{2}h°C as defined in the following equation, are shown in Figures 11 and 12 for the cooling and heating case, respectively.

$$\alpha_c = q / (\theta_w - \theta_{ave})$$

where, θ_w is wall surface temperature and θ_{ave} is volumetric mean temperature of room air.

The heat flow distribution of ceiling is fairly uniform, taking values of 10 kcal/m^{2}h in the heating

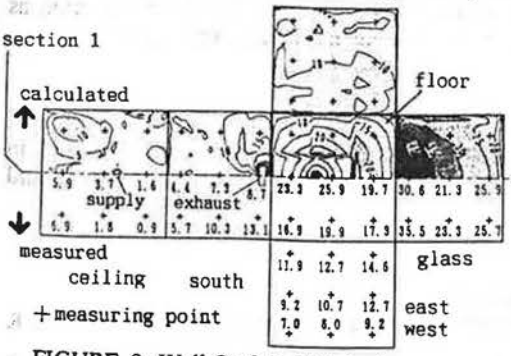

FIGURE 9 Wall Surface Distribution of Convective Heat Flows (C10, Type 3, Mesh 3, dimensions in kcal/m^{2}h)

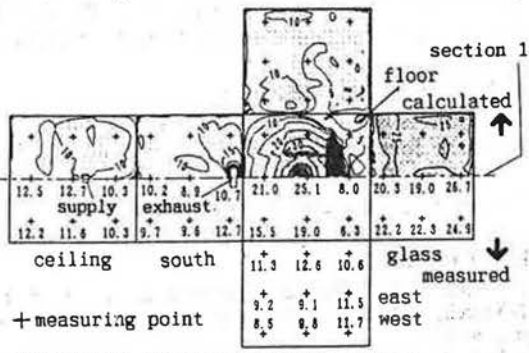

FIGURE 10 Wall Surface Distribution of Convective Heat Flows (H12, Type 3, Mesh 3, dimensions in kcal/m^{2}h)

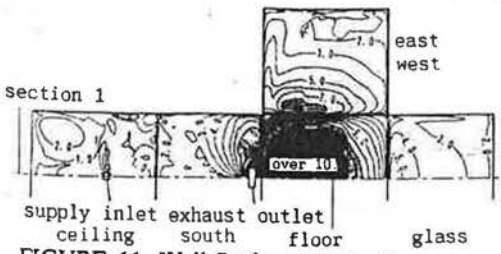

FIGURE 11 Wall Surface Distribution of Convective Heat Transfer Coefficients (C10, Type 3, Mesh 3, dimensions in kcal/m^{2}h°C)

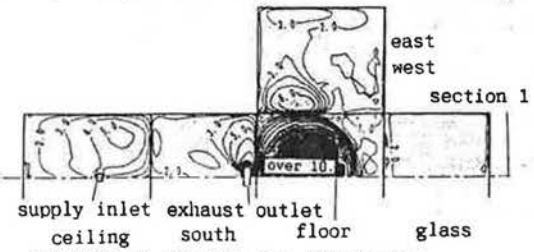

FIGURE 12 Wall Surface Distribution of Convective Heat Transfer Coefficients (H12, Type 3, Mesh 3, dimensions in kcal/m^{2}h°C)

case and much smaller values in the cooling case, typically 3 kcal/m^{2}h. These differences are responsible for the heat flow direction as mentioned earlier. In the vertical insulated walls, lower portions take larger heat flows than the upper portions, being affected by the radial wall jet formed close to the floor. The heat flow distribution in the glass surface is nearly uniform in the heating case, which is characteristic of natural convection over a cold plate. In the cooling case, however, the radial wall jet reaches the glass surface so the lower portion takes larger heat flow. Nearly circular heat flow contours are observed in the floor irrespective of the heating and cooling cases, and the largest values occur near the center of jet impinging. The results of calculations show satisfactory agreement with the corresponding experiment data.

Calculated convective heat transfer coefficient α_c for the ceiling is typically 1.0 kcal/m^{2}h°C in the cooling case, and is much smaller than in the heating case. It ranges from 2.0 to 5.0 kcal/m^{2}h°C. α_c in the vertical walls, including the glass surface, taking larger values in the cooling case than in the heating case especially in the lower portion of walls. The extremely large α_c near the exhaust outlet probably originates from the poor representation of the normal turbulent stress inherent in the k–ε turbulence model. This problem is to be overcome by changing to a more sophisticated turbulence model. Almost constant distribution is observed on the glass surface in the heating case, reflecting uniform heat flow distribution. α_c on the floor decreases with distance from the jet impinging center, and the cold draught in the heating case results in markedly small α_c in the vicinity of the glass surface.

Although the limited number of measuring points preclude detailed comparison, the simulated α_c distribution appears consistent with the present experiments and other available data.

CONCLUSION

Numerical simulation of air distribution and wall heat flows of an air-conditioned heating and cooling room was conducted by means of the k–ε turbulence model and wall functions. The preliminary simulation based on the imposed wall heat flows shows the fundamental applicability of the turbulence model to buoyancy-affected indoor airflows. Three types of wall functions were tested for predicting wall heat flows, and the results produced by the wall function which depends on turbulence energy at wall adjacent node and takes account of viscous sublayer thickness (Type 3) are in the most satisfactory agreement with the corresponding experiments. These suggest the strong possibility of accurate numerical prediction of indoor air distribution as well as wall heat flows with a proper combination of turbulence model and wall function.

ACKNOWLEDGEMENTS

The authors wish to express their gratitude to Mr. Togari and Mr. Akiba of Kajima Technical Research Institute for their great help during the experiments. This study has been sponsored in part by the Grant-in Aid for Scientific Research from the Ministry of Education, Science and Culture of Japan, and Tokyo Gas, Inc.

REFERENCES

1) Viollet, P. 1987. Nuclear engineering and design 99, pp.365–377.
2) Viecelli, J. A. 1971. A computing method for incompressible flows bounded by moving walls, J. Comput. Phys. 8, pp.119–143.
3) Patel, V. C.; Rodi, W.; Scheuerer, G. 1984. Turbulence models for near-wall and low Reynolds number flows; A Review, AIAA Journal, vol.23, No.9.
4) Gebhalt, B. 1959. A new method for calculating radiant exchanges, ASHRAE Trans., vol.65.
5) Kaizuka, M.; Kajiya, R. 1983. A numerical study on the prediction method of room air distribution applying to natural convection from a vertical heated plate, Proc. annual meeting of A.I.J. (Architectural Institution of Japan), pp.427–428 (in Japanese).
6) Kurabuchi, T.; Kamata, M. 1989. Wall boundary conditions of numerical method of non-isothermal indoor airflow – natural convection on a vertical heated plate – , Proc. annual meeting of SHASE (The Society of Heating, Air-conditioning, and Sanitary of Japan), pp.565–568 (in Japanese).
7) Launder, B. E.; Spalding, D. B. 1974. The numerical computation of turbulent flows, Comput. methods Appl., Mech. Engng. 3, P269–289.
8) Chieng, C. C.; Launder, B. E. 1980. On the calculation of turbulent heat transport downstream from an abrupt pipe expansion, Numerical Heat Transfer, vol.3.
9) Takemasa, Y.; Kurabuchi, T.; Kamata, M. 1990. Wall boundary conditions of numerical method of indoor airflow – natural convection near a vertical heated flat plate – , Proc. annual meeting of A.I.J., pp.485–486 (in Japanese).